

The Effect of the Third Element Cr on Oxidation Behavior of Fe-xCr-10Al (at.%) Alloys at 900°C

Z.G. Zhang^{*,a,b}, X.L. Zhang^b, L. Sheng^b and X. Teng^b

^aState Key Laboratory for Corrosion and Protection, Institute of Metal Research, Chinese Academy of Sciences, Wencui Road 62, 110015, Shenyang, China

^bDepartment of Applied Chemistry, Shenyang Institute of Chemical Technology, 110142, Shenyang, China

Abstract: Alloys Fe-(0, 5, 10)Cr-10Al (all in at.%) were oxidized at 900°C in 1 atm oxygen to study the effect of Cr additions on the oxidation behavior. The oxidation kinetics was recorded with a thermal microbalance. The morphologies and microstructures of the oxide scales were examined using SEM, EDS, and XRD. Fe-10Al developed an Al₂O₃-rich scale during the initial stage of oxidation, and a non-protective scale containing oxides of Fe and Al formed. Mixed oxides of Al and Fe formed firstly on Fe-5Cr-10Al, but an externally dense and continuous Al₂O₃-rich scale formed. The initially formed Fe oxides were locally reduced to Fe-rich particles. Fe-10Cr-10Al formed an Al₂O₃-rich scale from the onset of oxidation and this slowly growing scale was protective up to 50 h. The Cr additions to Fe-10Al were beneficial for restraining the oxidation of Fe, but that did not promote the transition from metastable Al₂O₃ to α -Al₂O₃.

Keywords: Iron-based alloys, high temperature oxidation, third element effect, metastable Al₂O₃.

INTRODUCTION

Iron-based alloys are commercially important high-temperature materials, among which the Fe-Al [1-7] and Fe-Cr-Al [7-17] alloys are of very great interest in the studies of high temperature oxidation. Fig. (1) schematically shows the oxide map of Fe-Al alloys, which directly correlates oxidation products with oxidation conditions. The data points in Fig. (1) were obtained during the oxidations performed in oxygen of 1 atm (0.1 MPa) or in air. Al₂O₃ forms more easily at higher temperatures. The oxygen pressure did not exert much effect on the scale development on Fe-Al when it was higher than 160 Torr (2.13×10⁴ Pa or 0.21 atm) [4], but lower oxygen pressure promoted formation of Fe oxides [18-20]. The existence of water vapor was reported to promote the growth of Fe-rich nodules [4] or to lead to internal oxidation [7].

Many oxidation studies of Fe-Cr-Al alloys have concentrated on those of commercial compositions. Fig. (2) is the isothermal oxide map, constructed by summarizing the results of relative papers, for the oxidation of Fe-Cr-Al alloys in oxygen of 1 atm or in air at 1000°C. Most of the alloys with commercial compositions are Al₂O₃ formers, and oxidant pressure did not affect the oxidation properties very much. A systematic study of the oxidation behavior of high-purity Fe-Cr-Al alloys, containing 0–27 wt.% Cr and 1–10 wt.% Al, at 800°C in oxygen of 200 Torr was carried out by Tomaszewicz and Wallwork [21]. Four major types of scaling behaviors were encountered, and an “oxide map” was constructed by superposing morphological features onto a phase equilibrium diagram at 800°C. Additions of Cr did not

reduce the concentration of Al, where the transition from a bulky, continuous, and stratified scale to a thin Al₂O₃ scale interspersed with Fe-oxide nodules occurred; however, the prevention of nodule growth was directly attributed to Cr additions [21]. A study on the cyclic oxidation, in oxygen at 1 atm over temperature 950–1050°C, of Fe-10wt.%Cr alloys containing 2–8 wt.% Al was carried out [22], both oxidation resistance and scale adhesion were improved with increasing Al content.

Addition of Cr to the binary Fe-Al alloys reduces the concentration of Al required to establish the Al₂O₃ scale [7, 8, 10, 11]. Fe-Cr-Al alloys offer an example of the so-called third element effect (TEE), by which the critical content of a most reactive component C needed to establish exclusive external scales of its oxide on ternary A-B-C alloys, where A is the most noble component, is reduced with respect to binary A-C alloys by the addition of an element B with an oxygen affinity intermediate between those of A and C [23]. The mechanism of TEE is not yet clear, but the explanations proposed so far, following the initial suggestion by Wagner [24], attribute the beneficial effect of B to its ability to induce a transition between the internal and external oxidation of C on ternary alloys under lower C levels than for binary A-C alloys [23]. The mechanism of the Cr effect on Fe-xCr-10Al (at.%) alloys is apparently different from those considered in the classical explanations of TEE because Fe-10Al does not suffer internal oxidation at high temperatures [2, 4]. Since this kind of TEE involving transition from external oxidation of both Fe and Al to exclusive oxidation of Al has not been the object of specific investigations, thus the oxidation behavior of the Fe-10at.%Al alloy with different Cr additions is studied by focusing on the Cr effect.

EXPERIMENTAL PROCEDURE

The alloys used in this investigation were prepared by vacuum arc-melting using appropriate mixtures of high pu-

*Address correspondence to this author at the Department of Applied Chemistry, Shenyang Institute of Chemical Technology, 110142, Shenyang, China; E-mail: zhg_syict@sohu.com

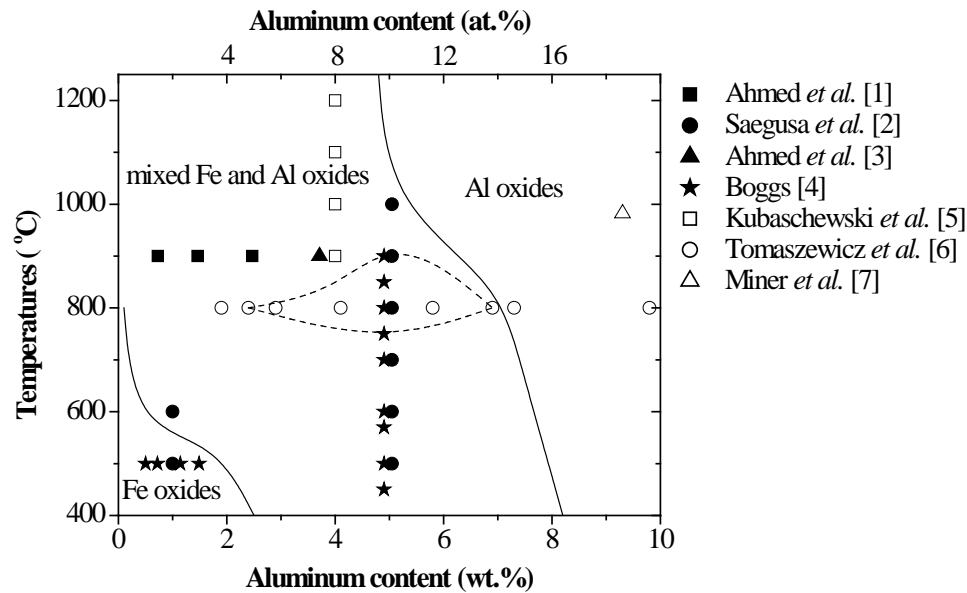


Fig. (1). Oxidation properties of Fe-Al alloys. Solid and open symbols present that the oxidations were carried out in 1 atm oxygen and in air, respectively.

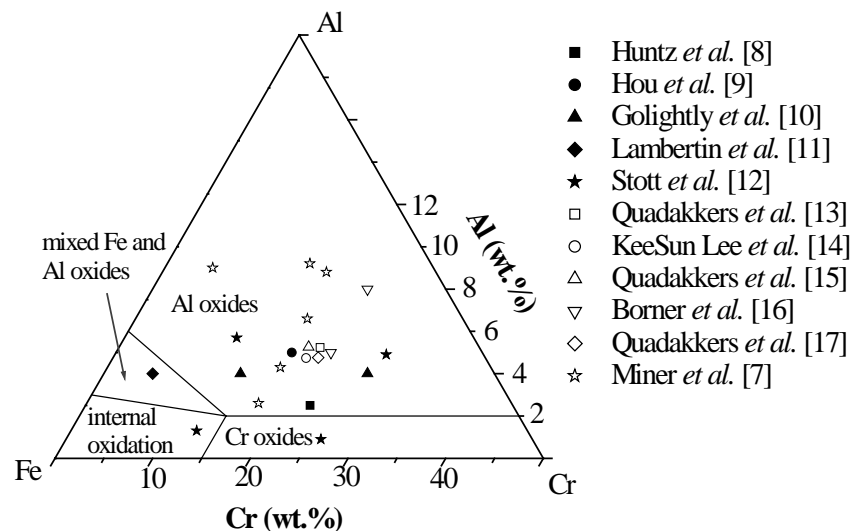


Fig. (2). Oxidation properties of Fe-Cr-Al alloys at 1000°C. Solid and open symbols present that the oxidations were carried out in 1 atm oxygen and in air, respectively.

rity metals (99.999 wt.%). After annealing at 1100°C in vacuum (below 10^{-7} atm) for 12 h, the finger-shaped ingots were cut into slices using a diamond saw. The elliptical slices were about 0.6 mm thick with limiting diameters of about 8 mm and 7 mm. A hole with diameter of 1 mm was drilled on each slice near the edge. The lateral face of every slice was firstly ground with coarse abrasive paper to remove the oxides probably formed during the annealing. For each specimen, the lateral face and the two sectioning faces were mechanically abraded on successively finer abrasive papers up to 1000 grit and 2000 grit, respectively. The specimens were successively cleaned with water, acetone, and ethanol, and then dried. Prior to cleaning, the dimensions of the specimens were measured for calculating the surface area.

The composition of each alloy was analyzed using energy dispersive spectroscopy (EDS). The nominal and the

actual compositions of the alloys in atom percent are listed in Table 1. The alloys in this study are always represented by nominal composition in atom percent.

Before oxidation, the specimen was suspended with quartz filaments, and the reaction chamber was flushed using sufficient oxygen. After the temperature reached 900°C, the vertical furnace was elevated to locate the specimen in the hot zone. It was a hermetical system with an inlet and an outlet of oxygen. The mass change of the specimen was continuously recorded with a thermal microbalance (SETARAM MTB 10-8).

The phase analysis was performed by X-ray diffraction (XRD, Rigaku D/max-2500pc). Surface morphologies of oxidation products were examined with a scanning electron microscope (SEM, Philips XL30). The specimen was mounted in a cold-setting epoxy resin for examining the

cross-section. EDS were used to determine distributions of elements in the various solid phases.

Table 1. Chemical Composition of the Experimental Alloys

Nominal	Analysis (at.%)		
	Fe	Al	Cr
Fe-10Al	90.2 <i>n</i> = 18, <i>s</i> = 0.69	9.8 <i>n</i> = 18, <i>s</i> = 0.69	-
Fe-5Cr-10Al	85.1 <i>n</i> = 18, <i>s</i> = 0.60	9.6 <i>n</i> = 18, <i>s</i> = 0.55	5.3 <i>n</i> = 18, <i>s</i> = 0.20
Fe-10Cr-10Al	80.1 <i>n</i> = 12, <i>s</i> = 0.55	9.6 <i>n</i> = 12, <i>s</i> = 0.60	10.3 <i>n</i> = 12, <i>s</i> = 0.31

Note: *n* presents measuring times, and *s* is standard deviation.

RESULTS

Oxidation Kinetics

The two ternary alloys, Fe-5Cr-10Al and Fe-10Cr-10Al, were oxidized at 900°C in 1 atm oxygen for both 10 h and 50 h respectively, whereas the alloy Fe-10Al underwent two 50 h runs. The mass gain curves of the 10 h runs were in rea-

sonable agreement with those of the starting stage of the 50 h runs. The mass gain curves of the three alloys are presented in Fig. (3); the corresponding parabolic plots are given in Fig. (4).

None of these curves adheres to a single parabolic relation. During the first 1.0 h, Fe-10Al showed a slow initial stage with a parabolic rate constant of about $1.9 \times 10^{-14} \text{ g}^2 \cdot \text{cm}^{-4} \cdot \text{s}^{-1}$, but this initial parabolic kinetics was immediately substituted by a linear kinetics corresponding to linear rate constant of about $4.7 \times 10^{-9} \text{ g} \cdot \text{cm}^{-2} \cdot \text{s}^{-1}$ until 50 h. In the first oxidation duration from about 0.4 to 2.0 h, Fe-5Cr-10Al showed an approximate linear stage with rate constant of about $4.9 \times 10^{-8} \text{ g} \cdot \text{cm}^{-2} \cdot \text{s}^{-1}$, after which the instantaneous parabolic rate constant promptly decreased, and after 4.7 h it became nearly constant up to the end. The Fe-10Cr-10Al had a low initial stage oxidation rate and then subsequently reached the second stage with rate constant of about $2.6 \times 10^{-14} \text{ g}^2 \cdot \text{cm}^{-4} \cdot \text{s}^{-1}$ from 5 h to 50 h.

Fe-10Cr-10Al had the lowest mass gain after 50 h oxidation, and the two successive parabolic rate constants were adjacent in value. For Fe-5Cr-10Al, the oxidation was very fast at initial stage, but slowing down during oxidation and eventually reached a very slow rate. The mass gain curve of alloy Fe-10Al seems a linear relationship (Fig. 3), and the

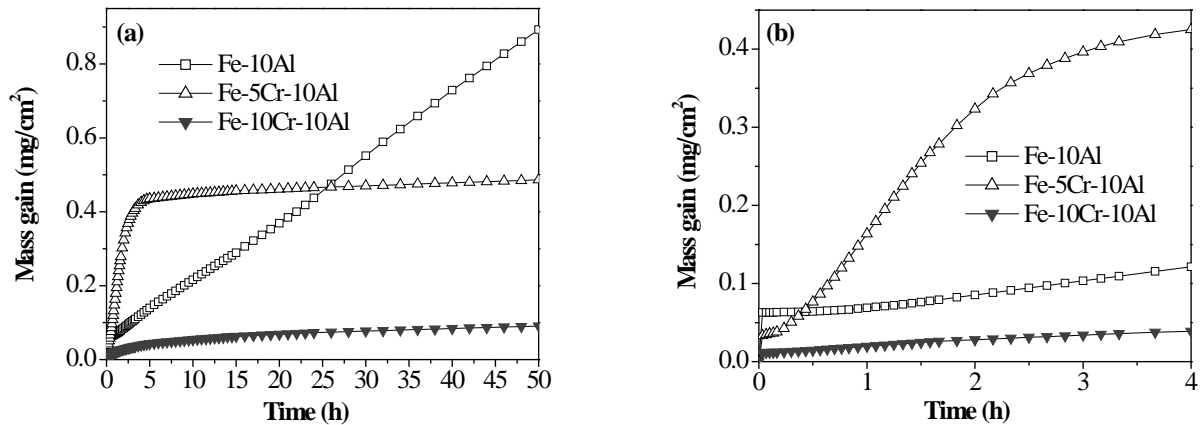


Fig. (3). Oxidation kinetics of Fe-10Al, Fe-5Cr-10Al, and Fe-10Cr-10Al at 900°C in 1 atm oxygen. (a) Plot for the total oxidation duration, (b) expanded plot for oxidation duration of the initial 4 h.

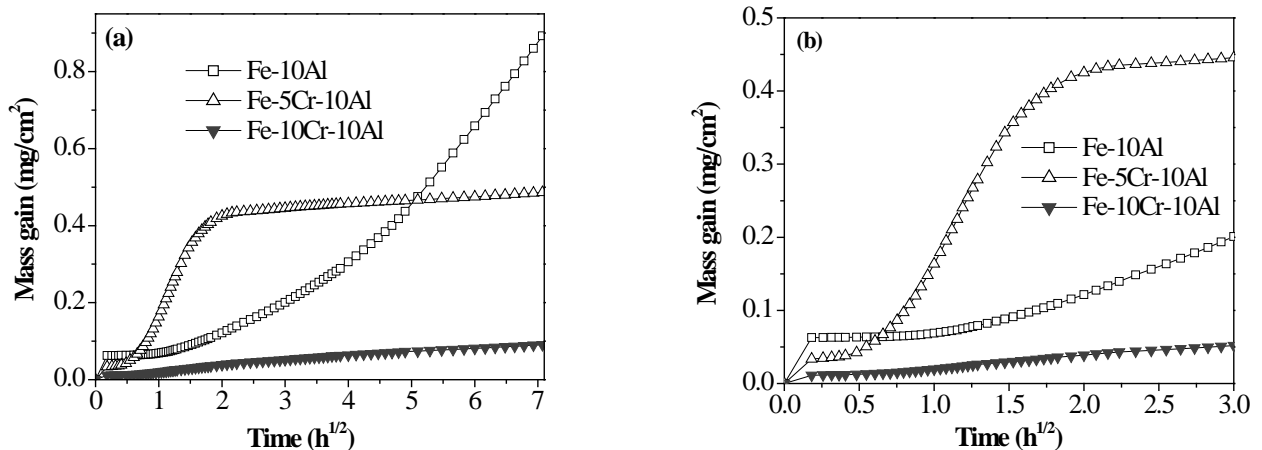


Fig. (4). Parabolic plots of oxidation kinetics of Fe-10Al, Fe-5Cr-10Al, and Fe-10Cr-10Al at 900°C in 1 atm oxygen. (a) Plot for the total oxidation duration, (b) expanded plot for oxidation duration of the initial 9 h.

mass gain steadily increased with oxidation time. Values of the parabolic rate constants for the initial and steady state stages of the three alloys are given in Table 2.

Table 2. Approximate Parabolic Rate Constants (k_p) for Oxidation at 900°C in 1 atm Oxygen

Alloy	Oxidation Duration (h)	k_p ($\text{g}^2\text{cm}^{-4}\text{s}^{-1}$)
Fe-5Cr-10Al	0.4 to 2.0	linear
	4.7 to 50	2.9×10^{-14}
Fe-10Cr-10Al	0.5 to 4.7	1.0×10^{-13}
	5 to 50	2.6×10^{-14}
Fe-10Al	0 to 1.0	1.9×10^{-14}
	1.0 to 50	linear

Morphology of Scales

Figs. (5, 6) show the surface and cross sectional morphologies, respectively, of alloy Fe-10Al after 50 h oxidation at 900°C in oxygen at 1 atm. The oxide scale was very wrinkling and occasionally localized Fe-rich nodules formed, while the cross section revealed that the scale was composed of mixed Al and Fe oxides. The XRD analysis (Fig. 7) indicated that this scale was a mixture of hematite (Fe_2O_3), $\alpha\text{-Al}_2\text{O}_3$, and a small amount of magnetite (Fe_3O_4).

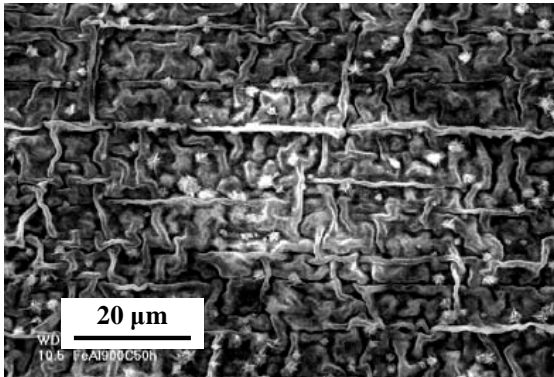


Fig. (5). Micrograph of surface morphology of oxides on Fe-10Al after 50 h oxidation at 900°C in 1 atm oxygen.

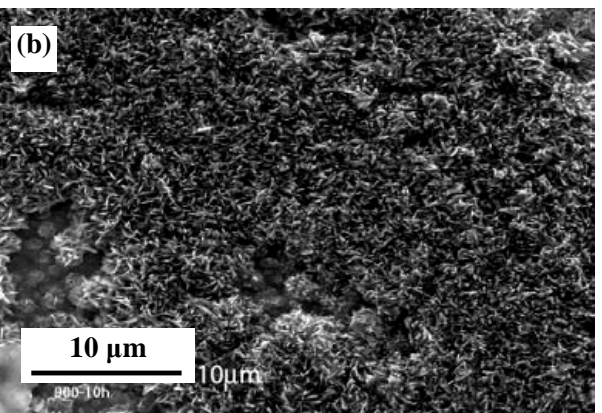
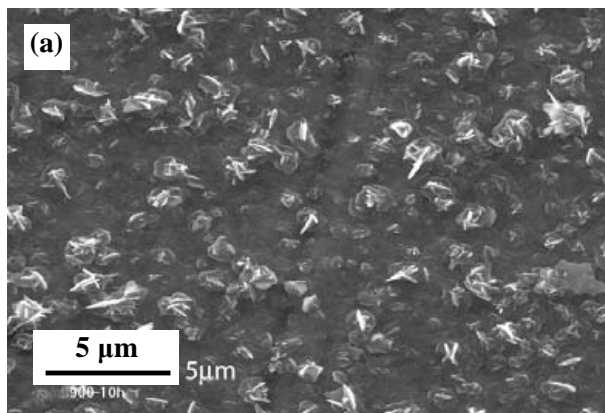


Fig. (8). Micrographs of surface morphology of oxides on Fe-5Cr-10Al after 10 h oxidation at 900°C in 1 atm oxygen. (a) General morphology, (b) morphology of plate-like structure.

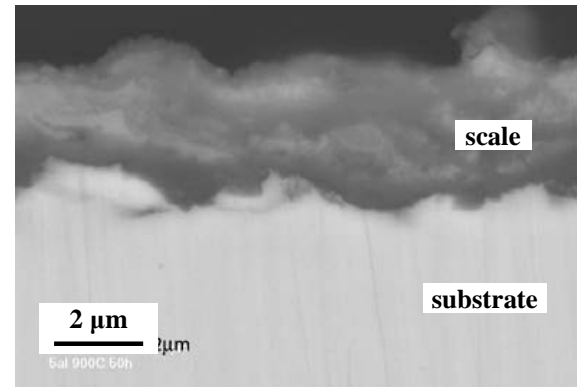


Fig. (6). Micrograph of cross section of Fe-10Al after 50 h oxidation at 900°C in 1 atm oxygen.

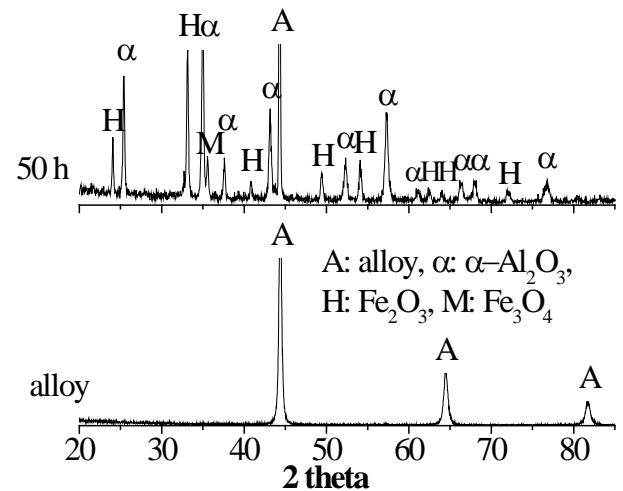


Fig. (7). XRD analysis of alloy Fe-10Al and oxides formed on the alloy after oxidation at 900°C in 1 atm oxygen.

The surface and cross sectional morphologies of alloy Fe-5Cr-10Al after 10 h oxidation are shown in Figs. (8, 9), respectively. Protrusions of Al-rich oxide distributed uniformly on the oxidized surface of the alloy, and no convolution of oxides was found (Fig. 8a). About 20% of the surface was covered by a layer of oxide with plate-like structure (Fig. 8b). In addition, many Fe oxide nodules formed on the specimen edge, and the nodules are much bigger than those on Fe-10Al. The cross sectional micrograph reveals the exist-

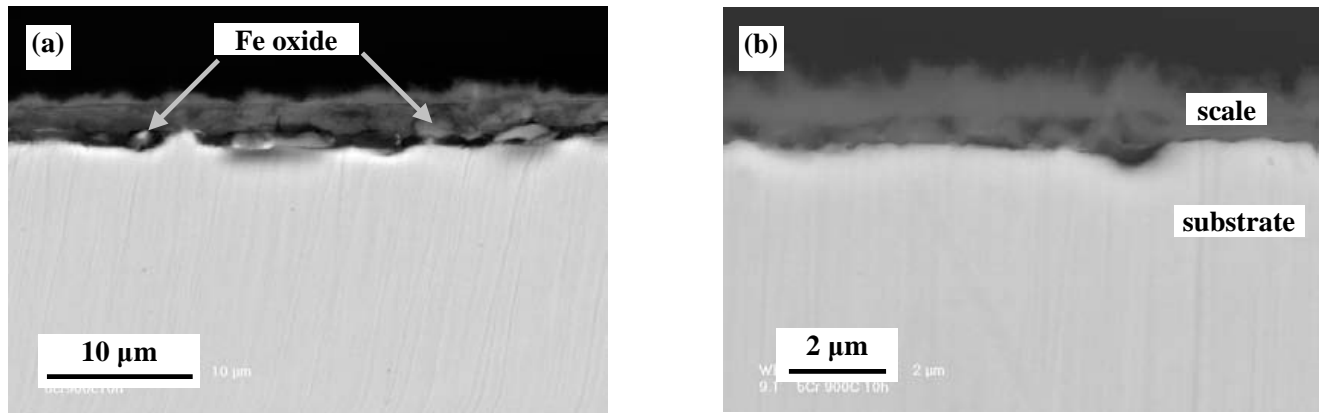


Fig. (9). Micrographs of cross sections of Fe-5Cr-10Al after 10 h oxidation at 900°C in 1 atm oxygen. (a) Morphology corresponding to Fig. (8a), (b) morphology corresponding to Fig. (8b).

tence of inclusions of Fe oxide (Fig. 9a). α -Al₂O₃, θ -Al₂O₃, and Fe₂O₃ were identified in the 10 h scales using XRD analysis (Fig. 10). After 50 h oxidation, the alloy developed a convoluted scale, and Fe oxide nodules are also found on the edge of the specimen (Figs. 11, 12). The existence of Fe₂O₃ was not identified with XRD analysis (Fig. 10) for the 50 h scales although parts of the scales contains small amount of Fe-rich oxides (Fig. 12b).

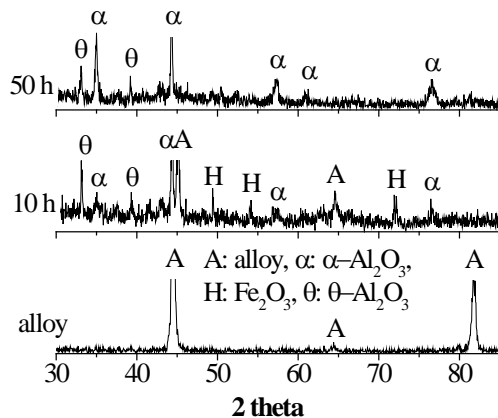


Fig. (10). XRD analysis of alloy Fe-5Cr-10Al and oxides formed on the alloy after oxidation at 900°C in 1 atm oxygen.

The micrographs of oxides formed on alloy Fe-10Cr-10Al after 10 and 50 h oxidation at 900°C in oxygen at 1 atm

are shown in Figs. (13, 14), respectively. The scale on the 10 h specimen was slightly convolute and the convolutions were much higher along the grain boundary of the alloy. The scale on the 50 h specimen was flatter than that on the 10 h specimen. More metastable Al₂O₃ formed after 50 h oxidation than after 10 h. Only α -Al₂O₃ was identified after 10 h oxidation whereas both α -Al₂O₃ and θ -Al₂O₃ were identified after 50 h oxidation (Fig. 15). The alloy did not form any Fe oxide nodules during the oxidation.

DISCUSSION

The additions of Cr to alloy Fe-xCr-10Al led to the transition of oxidation kinetics, i.e. from linear relationship (Fe-10Al) to parabolic relationship during steady oxidation stage (Fe-5Cr-10Al), and then to parabolic relationship during whole oxidation stage (Fe-10Cr-10Al).

The alloy Fe-10Al formed a convoluted and layered scale after 50 h oxidation at 900°C. The XRD analyses indicated that the oxides are mixtures of α -Al₂O₃ and Fe₂O₃, but a small amount of Fe₃O₄ was also detected. The XRD pattern for the 50 h scale shows a strong component from the alloy substrate (Fig. 7). Al₂O₃ or Al₂O₃-rich oxides formed during the initial stage of oxidation, which was corresponding to the parabolic rate constant, $1.9 \times 10^{-14} \text{ g}^2 \cdot \text{cm}^{-4} \cdot \text{s}^{-1}$, of the typical value for the growth of Al₂O₃ on Al-containing alloys [25] at 900°C. However, the slow-growing scale was replaced later by a layered scale containing mixtures of Fe and Al oxides.

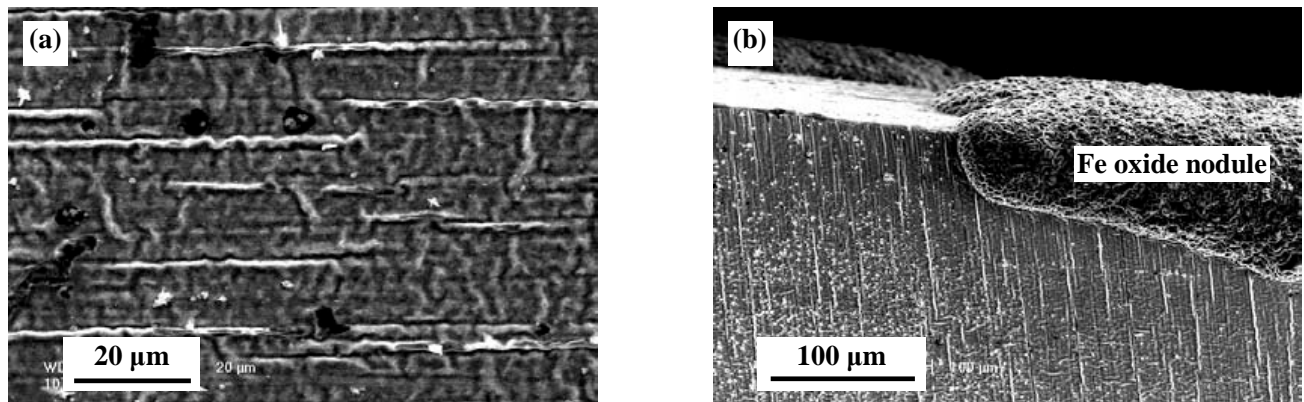


Fig. (11). Micrographs of surface morphology of oxides on Fe-5Cr-10Al after 50 h oxidation at 900°C in 1 atm oxygen. (a) General morphology, (b) morphology of Fe oxide nodules formed on the specimen edge.

Because only a few localized Fe-rich nodules formed, the formation of these nodules did not play an apparent role on the total mass gain during oxidation. The formation of Fe-rich nodules has been noted in several investigations on the oxidation of binary Fe-Al alloys [2, 4, 6]. It seems that the nodules apt to form on the alloys containing 3–6 wt.% Al at temperatures 750 to 900°C, as presented by the loop of dashed line in Fig. (1). The nodular formation was suggested to result from the depletion of Al beneath the cracks in the Al_2O_3 film [4]. There should be other factors responding to the formation of oxide nodules, such as the corner effects [2], composition of oxidant [4], and surface conditions of the specimens. The present authors have studied the roughness effects on the oxidation properties of Fe-xCr-10Al alloys containing 0–10 at.% Cr [26], and the results indicated that the alloy surface conditions played important roles on the formation of nodular Fe-rich oxides.

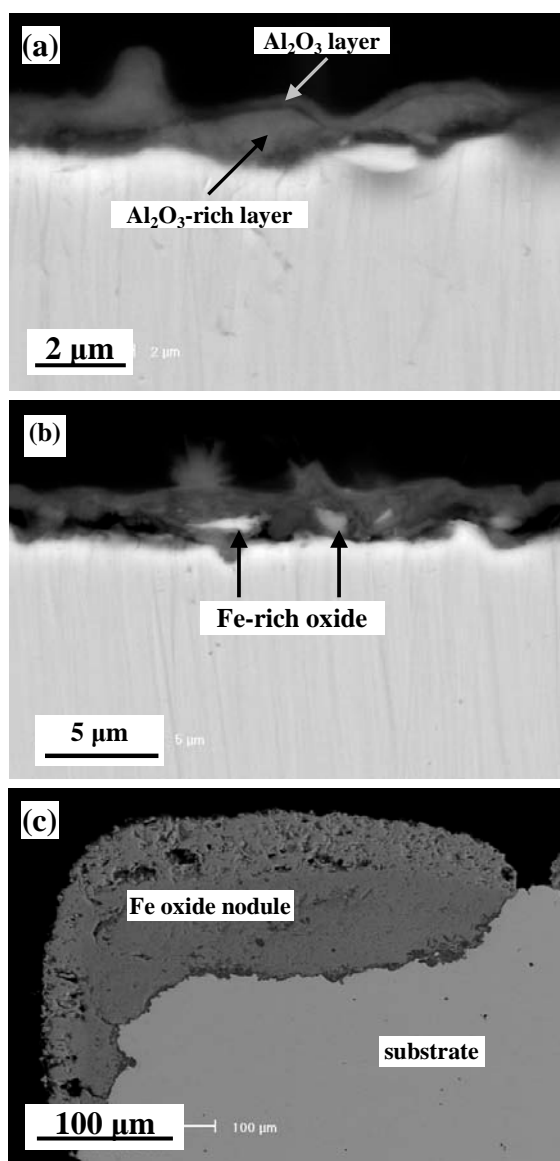


Fig. (12). Micrographs of cross sections of Fe-5Cr-10Al after 50 h oxidation at 900°C in 1 atm oxygen. (a) General morphology, (b) local morphology, (c) morphology of a Fe oxide nodule formed on the specimen edge.

Duplex or triplex scales were found to form on Fe-Al alloys after oxidation at high temperatures [1-3]. The cross section of the oxidized Fe-10Al alloy revealed that layered scales composed of the mixture oxides of Fe and Al were developed during the oxidation. It seems that the alloy Fe-10Al developed an Al_2O_3 or Al-rich scale during the initial stage of oxidation. However, this initial scale was not thick and dense enough, and some cracks and/or defects occurred. The Al oxide and Fe oxide formed alternately after the initial oxidation stage, and the stratified scale became thick steadily. Although the oxidation rate may present local fluctuations, the average kinetics may become reasonably regular presented by a linear relationship (Fig. 3).

The compound $\text{Fe}_2\text{O}_3\cdot\text{Al}_2\text{O}_3$ (FeAlO_3) is known to be stable only at temperatures above 1300°C [27], so there should be no FeAlO_3 in the layered scales on Fe-10Al. However, the existence of magnetite (Fe_3O_4) is expectable [4], and the spinel phase FeAl_2O_4 maybe exists due to the reaction between Fe_3O_4 and Al_2O_3 [6], but the Fe-Al-O equilibrium oxygen pressure diagram at 900°C [28] illustrated that the spinel phase could exist only at oxygen pressure below 1.4×10^{-8} atm. Therefore, the content of Fe_3O_4 and FeAl_2O_4 is probably lower than the detection limit, but a weak diffraction peak of Fe_3O_4 was found (Fig. 7).

The kinetics of Fe-5Cr-10Al at 900°C is presented by a fast linear oxidation during initial stage, and the oxidation rate was rapidly decreased at middle stage, and then a slow parabolic oxidation reached at final stage. The growth rate of Fe-rich nodules is very rapid because of their huge volume in comparison with the scale thickness, but their growth was undercut by an Al_2O_3 -rich healing layer with time (Fig. 12c). Since the oxide of Cr was not detected, the fast oxidation during initial stage is attributed to the simultaneous growth of oxides of Fe and Al, especially the formation of Fe-oxide nodules on the specimen edge.

The surface morphologies of the scales formed on Fe-5Cr-10Al after 10 h reveals that around 20% of the area was covered by fast-growing θ - Al_2O_3 (in comparison with α - Al_2O_3). The other parts of the alloy surface uniformly developed outwards growing Al_2O_3 protrusions (Fig. 8a), which did not coalesce into an integral Al_2O_3 layer. The development of plate-like structure and protrusions suggested outwards transport of cations. However, the scales displayed convolute top-view morphology after 50 h, and the oxide with plate-like structure disappeared (Fig. 11a). The cross-sectional morphology after 50 h indicates most of the alloy surface was covered by a duplex scale composed of an outer Al_2O_3 layer and an inner Al-rich layer (Fig. 12a). The Al_2O_3 protrusions (Figs. 8a, 9a) have coalesced into a dense and integral scale, i.e. the outer Al_2O_3 layer. The plate-like structures or whiskers of metastable Al_2O_3 (θ - Al_2O_3) could be transformed to the α -crystal structure with the oxidation time. The thickness of the scales did not increase much with time from 10 h to 50 h, which was consistent with the kinetics of the second stage. The XRD analysis did not identify the existence of Fe_2O_3 in the 50 h scale as it did for the 10 h scale (Fig. 10), so the content of Fe_2O_3 of the 50 h scale should be lower than the detection limit, which implied that Fe got much less opportunity to form Fe oxide than Al did during the oxidation time from 10 h to 50 h. Since the XRD pattern from the substrate was not detected (Fig. 10), it is

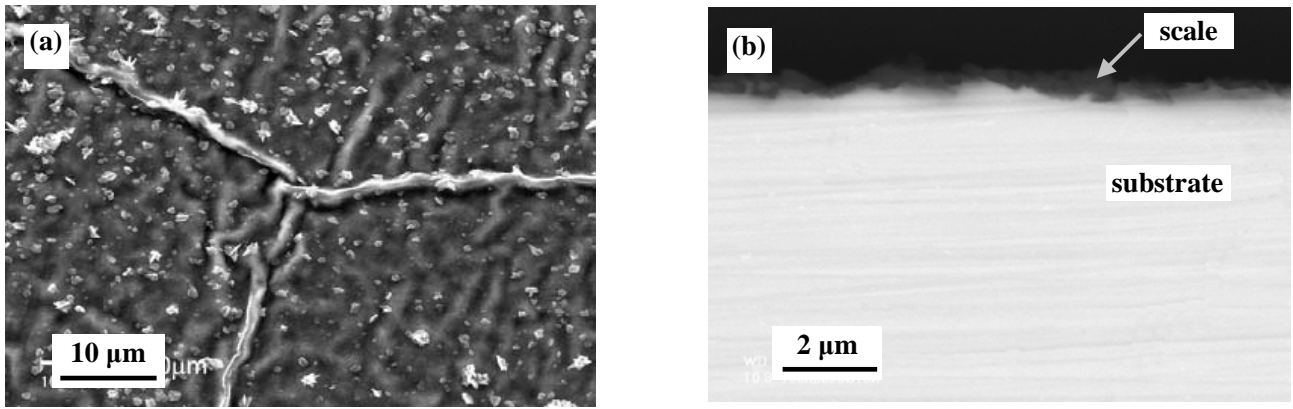


Fig. (13). Micrographs of the scales formed on Fe-10Cr-10Al after 10 h oxidation at 900°C in 1 atm oxygen. (a) Surface morphology, (b) cross section.

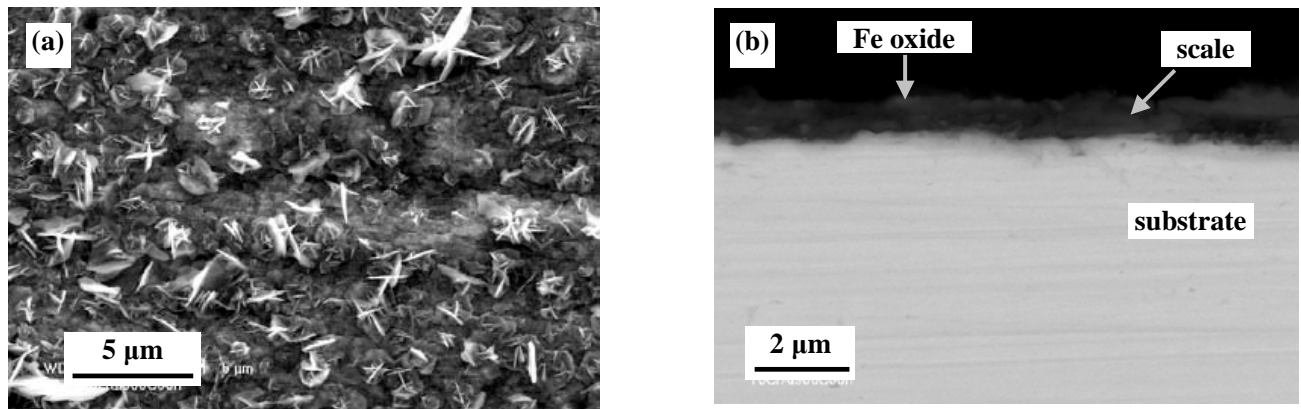


Fig. (14). Micrographs of the scales formed on Fe-10Cr-10Al after 50 h oxidation at 900°C in 1 atm oxygen. (a) Surface morphology, (b) cross section.

probably that the existence of small amount of Fe oxide near the scale/substrate interface was not identified. However, Al_2O_3 is the prevailing oxide formed on Fe-5Cr-10Al after a transient oxidation period in which the alloy components, mainly including Fe and Al, were simultaneously oxidized. Fe-5Cr-10Al is more sensitive than Fe-10Al to surface conditions of the investigated alloys for the Fe-oxides nodules formation during initial stage oxidation [26]. Therefore, the Cr addition at level of about 5 at.% to binary Fe-Al alloy restrained the growth of Fe oxides after a transient stage despite it actually promoted the simultaneous oxidation of Fe and Al in the initial stage of oxidation (in comparison with Fe-10Al).

It is not possible for Al and/or Cr to reduce the Fe oxides when the oxygen pressure is higher than the decomposition pressure of Fe oxides. However, the existence of inclusions that are very rich in Fe but poor in oxygen (Fig. 12b) implies that localized displacement reaction between Al (or Cr) and Fe oxide occurred, and the oxygen pressure at such locations is lower than the decomposition pressure of Fe oxide.

The alloy Fe-10Cr-10Al formed a protective Al_2O_3 -rich scale during the oxidation at 900°C, which is in agreement with the parabolic oxidation kinetics shown in Table 2. However, the scale formed at 900°C was not as dense and integral as that formed at 1000°C [29] after corresponding oxidation time. There existed a small amount of Fe-containing oxide on the gas/scale interface (Fig. 14b), which

was not identified by the XRD analysis (Fig. 15) because of the low content. The scale after 50 h became flatter than that after 10 h oxidation and more metastable Al_2O_3 formed; the surface morphology was consistent with the results of XRD analysis. The parabolic rate constant of about $10^{-14} \text{ g}^2 \cdot \text{cm}^{-4} \cdot \text{s}^{-1}$ is characterized by the Al_2O_3 formation at 900°C [25], so the k_p about ten times big as the typical value during the first oxidation stage (Table 2) is attributed to the formation of the Al-rich oxides containing Fe from the onset of the oxidation. The formation of oxide whiskers was due to the outwards diffusion of Al.

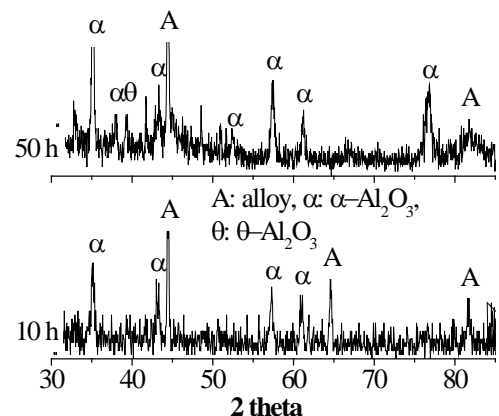


Fig. (15). XRD analysis of oxides formed on alloy Fe-10Cr-10Al after oxidation at 900°C in 1 atm oxygen.

Metastable Al_2O_3 ($\theta\text{-Al}_2\text{O}_3$) was identified on both Fe-5Cr-10Al and Fe-10Cr-10Al using XRD analysis but not on Fe-10Al, which indicated that addition of Cr to Fe-Al could not have promoted the transition from $\theta\text{-Al}_2\text{O}_3$ to $\alpha\text{-Al}_2\text{O}_3$. This is not in agreement with has been proposed that addition of Cr promotes such a transition [20]. The reason is probably that Al_2O_3 is easier to form under Cr existence, and the transition from $\theta\text{-Al}_2\text{O}_3$ to $\alpha\text{-Al}_2\text{O}_3$ was not finished within the oxidation duration.

CONCLUSION

The oxidation of alloys Fe-(0, 5, 10)Cr-10Al (all in at.%) has been carried out at 900°C in 1 atm oxygen. Fe-10Al developed an Al_2O_3 -rich scale during the initial stage of oxidation, and a non-protective scale containing oxides of Fe and Al formed. Mixed oxides of Al and Fe formed firstly on Fe-5Cr-10Al, but an externally dense and continuous Al_2O_3 -rich scale finally developed. Fe-10Cr-10Al formed protective Al_2O_3 -rich scale from the onset of oxidation and this slowly growing scale was protective up to 50 h. The Cr additions to Fe-10Al promoted transition from the formation of external scale composed of Fe and Al oxides to the formation of protective Al_2O_3 -rich scale, but that did not promote the transition from metastable Al_2O_3 to $\alpha\text{-Al}_2\text{O}_3$.

ACKNOWLEDGEMENT

A financial support by the NNSF of China under the research projects nos. 50071058 and 50271079 is gratefully acknowledged.

REFERENCES

- [1] Ahmed HA, Smeltzer WW. Oxidation properties of Fe-Al alloys (1.5-5 a/o Al) in oxygen at 1173K. *J Electrochem Soc* 1986; 133: 212-6.
- [2] Saegusa F, Lee L. Oxidation of iron-aluminum alloys in the ranges 500-1000°C. *Corrosion* 1966; 22: 168-77.
- [3] Ahmed HA, Underhill RP, Smeltzer WW, Brett ME, Graham MJ. The use of mossbauer and auger spectroscopy for analysis of oxide layers on Fe-Al alloys. *Oxid Met* 1987; 28: 347-51.
- [4] William EB. The oxidation of iron-aluminum alloys from 450°C to 900°C. *J Electrochem Soc* 1971; 118: 906-13.
- [5] Kubaschewski O, Hopkins BE. *The oxidation of metals and alloys*. Butterworths: London; 1962.
- [6] Tomaszewicz P, Wallwork GR. Observations of nodule growth during the oxidation of pure binary iron-aluminum alloys. *Oxid Met* 1983; 19: 165-85.
- [7] Miner RG, Nagarajan V. The morphology of oxidation of alumina-forming iron-base alloys containing chromium and aluminum. *Oxid Met* 1981; 16: 313-25.
- [8] Huntz AM, Abderrazik GB, Moulin G, Young EWA, De Wit JHW. Yttrium influence on the alumina growth mechanism on an $\text{FeCr}_{23}\text{Al}_5$ alloy. *Appl Surf Sci* 1987; 28: 345-66.
- [9] Hou PY, Stringer J. Oxide scale adhesion and impurity segregation at the scale/metal interface. *Oxid Met* 1992; 38: 323-45.
- [10] Golightly FA, Wood GC, Stott FH. The early stages of development of $\alpha\text{-Al}_2\text{O}_3$ scales on Fe-Cr-Al and Fe-Cr-Al-Y alloys at high temperature. *Oxid Met* 1980; 14: 217-34.
- [11] Lambertin M, Stoklosa A, Smeltzer WW. Oxidation properties of Fe-5Cr-4Al (wt.%) in oxygen at temperature 1000 °C-1320 °C. *Oxid Met* 1981; 15: 355-73.
- [12] Stott FH, Wood GC, Hobby MG. A comparison of the oxidation behavior of Fe-Cr-Al, Ni-Cr-Al, and Co-Cr-Al alloys. *Oxid Met* 1971; 3: 103-13.
- [13] Quadackers WJ, Holzbrecher H, Briefs KG, Beske H. Differences in growth mechanisms of oxide scales formed on ODS and conventional wrought alloys. *Oxid Met* 1989; 32: 67-88.
- [14] Lee KS, Oh KH, Park WW, Ra HY. Growth of α -alumina oxide film in high temperature oxidation of Fe-20Cr-5Al alloy thin strip. *Scripta Mater* 1998; 39: 1151-5.
- [15] Quadackers WJ, Elschner A, Speier W, Nickel H. Composition and growth mechanisms of alumina scales on FeCrAl-based alloys determined by SNMS. *Appl Surf Sci* 1991; 52: 271-87.
- [16] Borner V, Emmerich K, Frolich K, Grabke HJ, Schmutzler HJ. High temperature oxidation behavior of rapidly solidified Fe-Cr-Al ribbons. *Mater Sci Eng* 1991; A134: 1062-4.
- [17] Quadackers WJ, Jedlinski J, Schmidt K, Krasovec M, Borchardt G, Nickel H. The effect of implanted yttrium on the growth and adherence of alumina scales on Fe-20Cr-5Al. *Appl Surf Sci* 1991; 47: 261-72.
- [18] Graham MJ, Eldridge JI, Mitchell DF, Hussey RJ. Anion transport in growing Cr_2O_3 and Al_2O_3 scales. *Mater Sci Forum* 1989; 43: 207-42.
- [19] Hickman JW, Gulberansen EA. An electron diffraction study of oxide films formed on alloys of iron, cobalt, nickel and chromium at high temperatures. *Trans Am Inst Min Metall Eng* 1947; 171: 344-70.
- [20] Hagel WC. The oxidation of iron, nickel, and cobalt-base alloys containing aluminum. *Corrosion* 1965; 21: 316-26.
- [21] Tomaszewicz P, Wallwork GR. The oxidation of high-purity iron-chromium-aluminum alloys at 800°C. *Oxid Met* 1983; 20: 75-109.
- [22] Sadique SE, Mollah AH, Islam MS, Ali MM, Megat MHH, Basri S. High-temperature oxidation behavior of iron-chromium-aluminum alloys. *Oxid Met* 2000; 54: 385-400.
- [23] Stott FH, Wood GC, Stringer J. The influence of alloying elements on the development and maintenance of protective scales. *Oxid Met* 1995; 44: 113-45.
- [24] Wagner C. Passivity and inhibition during the oxidation of metal at elevated temperatures. *Corros Sci* 1965; 5: 751-64.
- [25] Hindam H, Whittle DP. Microstructure, adhesion, and growth kinetics of protective scales on metals and alloys. *Oxid Met* 1982; 18: 245-84.
- [26] Zhang ZG, Hou PY, Gesmundo F, Niu Y. Effect of surface roughness on the development of protective Al_2O_3 on Fe-10Al (at.%) alloys containing 0-10 at.% Cr. *Appl Surf Sci* 2006; 253: 881-8.
- [27] Prescott R, Graham MJ. The oxidation of iron-aluminum alloys. *Oxid Met* 1992; 38: 73-87.
- [28] Elrefaie FA, Smeltzer WW. Thermodynamics of the system iron-aluminum-oxygen between 1073 K and 1573 K. *Metall Trans* 1983; 14B: 85-93.
- [29] Zhang ZG, Gesmundo F, Hou PY, Niu Y. Criteria for the formation of protective Al_2O_3 scales on Fe-Al and Fe-Cr-Al alloys. *Corros Sci* 2006; 48: 741-65.

Received: November 14, 2008

Revised: January 12, 2009

Accepted: January 16, 2009

© Zhang *et al.*; Licensee *Bentham Open*.

This is an open access article licensed under the terms of the Creative Commons Attribution Non-Commercial License (<http://creativecommons.org/licenses/by-nc/3.0/>) which permits unrestricted, non-commercial use, distribution and reproduction in any medium, provided the work is properly cited.